Estimation of evapotranspiration through an improved daily global solar radiation in SEBAL model: a case study of the middle Heihe River Basin

Jingqiu Yin[1], Xinfa Qiu[1], Shoubo Li[1], Guoping Shi[1], Huiyu Liu[2]

[1]College of Geography Science, Nanjing University of Information Science & Technology, Nanjing, China

[2]College of Geography Science,Nanjing Normal University,Nanjing,China

Correspondence to: Jingqiu Yin (autumn4001@126.com)

Abstract: The agricultural activities, hydrologic cycle, and ecological environment are seriously influenced by evapotranspiration (ET), especially in arid and semi-arid areas. A new method for estimating daily global solar radiation (GSR) over rugged terrains in the middle Heihe River Basin is developed on the basis of Iqbal model C. And with the land surface parameters retrieved from multisource remote sensing data, a daily surface ET on June 21–24, 2009, is simulated by using surface energy balance algorithm for land (SEBAL) model. The results show:

1. An improved daily GSR with a resolution of 100 m×100 m is implemented. The mean absolute bias error (MABE) is 9 W/m^2, and the mean absolute relative bias error (MARBE) is 2.5%. The MABE of the daily GSR using the SEBAL model is 122.2 W/m^2, and the MARBE is 33.9%.

2. The spatial distribution of the daily GSR is more reasonable using the improved model than the original model. The GSR is larger on a sunny slope (an open place) than on a shady slope (a rugged place).

3. Bringing the new model into SEBAL significantly improves the accuracy of the ET. The MABE of ET decreases from 2.1 mm (original scheme) to 0.6 mm (improved scheme),

26 and the MARBE declines from 44% to 13% accordingly. Moreover, the spatiotemporal

27 resolution of the ET simulation is effectively improved by the combined moderate-resolution

28 imaging spectroradiometer and thematic mapper surface parameters.

29 4. All highest ET value appeared in all types of water bodies, followed by farmland,

30 forest, wetland, and residential areas, the lowest values appeared over bare rock land. The

31 water consumption in these areas is dominated by agriculture. The new results provide better

32 theoretical basis and scientific guidance for ecosystem protection and sustainable utilization

33 of water resources.

34

1. Introduction

36 About 60% of global precipitation is consumed by evapotranspiration (ET),

37 while 99% of water in farmland system is consumed by ET (Kit, 2000). As an

38 important part of water cycle, ET is of great significance for understanding the water

39 cycle process, regulating the hydrological process by vegetation, and rational

40 utilization of limited water resources (Sellers et al., 1996), especially in arid and

41 semi-arid areas. Therefore, the accurate determination and estimation of the daily ET

42 can satisfy the requirements of not only agricultural production but also other

43 ecological water requirements and provide scientific guidance for the rational

44 utilization and distribution of water resources (Nie et al., 2004; Rahman et al., 2016),

45 especially during the growing season when numerous water resources are exhausted

46 in the middle reaches of the Heihe River Basin in China.

47   Surface energy balance algorithm for land (SEBAL) model (Bastiaanssen et al.,

48 1998a and 1998b) is currently a common method to estimate water and heat fluxes.

49 Using remote sensing data and meteorology knowledge, calculating water and heat

50 fluxes on a daily scale is feasible and widely applied (Bastiaanssen et al., 2000;

51 Teixeira et al., 2009; Liu, 2008; Yin, 2014; Li et al.,, 2010; Ahmad et al.,,2014;

52 Usman et al., 2015) . Liu (2008) verified that the SEBAL model is sensitive to daily

53 global solar radiation (GSR). Therefore, the daily GSR is an important input

54 parameter for ET estimation using the SEBAL model.

55   The solar radiation that reaches the ground is affected by astronomical,

56 atmospheric (i.e., air molecules, water vapor, and cloud), and surface factors (i.e.,

57 slope, aspect, terrain shading, and surface coverage). Thus, the simulation of GSR in a

58 rugged terrain is significantly complex (Zeng et al., 2005; Yeom et al., 2016; Shi et al.,

59 2018). Geographical information system (GIS) and remote sensing techniques have

60 provided new methods for estimating solar radiation, including the above mentioned

61 factors. Digital elevation model (DEM) data have been extensively used to simulate

62 solar radiation in mountainous areas (Williams et al., 1972; Bocquet, 1984; Dozier

63 and Frew, 1990; Qiu et al., 2003; Chen et al., 2013; Shi et al., 2018). However,

64 research on the daily GSR is limited to accurately estimate climatic factors on a

65 daily scale. Chen et al., (2013) developed a DEM-based radiation model to estimate

66 instantaneous clear-sky solar radiation for surface energy balance system to obtain

67 accurate energy absorbed by the mountain surface. However, terrain shading is

68 insufficiently considered. Shi et al., (2018) used Iqbal model C (1983) and DEM to

estimate the daily GSR to investigate the effects of topography. The daily GSR was acquired in a relatively coarse grid of 1 km×1 km. However, their method was not applied to a high spatiotemporal resolution estimation of the GSR directly, thereby making the performance of agriculture activities infeasible.

In the present study, a distributed model for daily GSR is proposed on the basis of possible solar radiation, which includes astronomical, atmospheric, and land surface factors in a relatively high spatiotemporal resolution. Based on the DEM data with 100 m resolution, weather station information (radiation, wind, and pressure), and remote sensing images of thematic mapper (TM) and moderate-resolution imaging spectroradiometer (MODIS), this study aims to 1) realize the estimation of daily GSR in a 100 m×100 m resolution, 2) compare and validate the estimated results with measured data, and 3) improve the application of simulated daily GSR by calculating ET using the SEBAL model.

2. Methodology

2.1. Study Area

The study area is located in the middle reaches of the Heihe River Basin in Northwestern China, including Linze County and Ganzhou District, with an elevation ranging from 1,360–3,600 m and an area of approximately 60,000 km2 (Fig. 1). An oasis is situated along the river, surrounded by a desert (Fig. 2). This area is typical warm temperate desert arid climate.

2.2. Data

2.2.1. Remote sensing data

Landsat TM data can provide high-resolution information about land surface temperature, land cover classification, albedo, normalized difference vegetation index(NDVI), and emissivity. This study adopts the Landsat TM5 image that was captured on June 24, 2009, in which the cloud cover in the study area was below 5% due to a favorable weather condition (Fig. 5a).

MODIS Levels 2 and 3 images on June 21–24, 2009, without clouds [cloud formation] are collected. NDVI, emissivity, and surface albedo are retrieved by using Level 2 products (500 m×500 m). Daily land surface temperature (LST) with a spatial resolution of 1 km comes [was adopted] from Level 3 MOD11A1.

2.2.2. Meteorological data

To supplement the TM [Landsat] and MODIS images, the heights of vegetation and the following meteorological data are required: air pressure, relative humidity, air temperature, sunshine duration, LST, wind speed, net radiation, and daily GSR. In addition, two ET measurements are placed in a farmland and a wetland station (Fig. 1). All the meteorological data must be measured hourly throughout the day.

2.2.3. GIS data

Considering the spatiotemporal resolution of remote sensing data, this study uses the DEM with a spatial resolution of 100 m×100 m and the vector map of the administrative boundary with the map scale of 1:250,000. All data are obtained from

the website of Digital Heihe (http://heihe.westgis.ac.cn). The land cover map is

created by a computer-assisted visual interpretation at the scale of 1:100,000 on the

basis of the TM image (Fig. 2).

2.3. Methodology

2.3.1. Improved daily GSR model

The daily GSR in the SEBAL model is calculated as follows (Bastiaanssen et al.,

1998a and 1998b; Chen et al., 2000):

$$R_{a24} = G_{sc} \times d_r \times \int_{\omega_1}^{\omega_2} \cos\theta d\omega, \tag{1}$$

where R_{a24} is the daily GSR, G_{sc} is the solar constant, that is, 1367W/m^2, d_r is the

earth-sun distance factor (dimensionless), ω_1 and ω_2 represent the solar hour angles

(radians) at 5 min after sunrise and at 5 min before sunset, respectively, and θ is the

solar zenith angle. $\cos\theta$ is calculated by Chen et al., method(2013).

In Eq. (1), only sun–earth spatial relations on a specific date, slope, and aspect

relations are considered. The effects of wet–clean air conditions and the terrain

shading are disregarded. The improved daily GSR model includes the above

mentioned factors, which can be categorized into two main models.

(1) Determination of GSR over a horizontal surface

The effects of air molecules, O_3, CO_2, oxygen, and other mixed gas and water

vapor on short-wave solar radiation are considered in this part by using Iqbal Model C.

A detailed description is presented in Shi et al., method (2018).

We obtain the daily global radiation under wet–clean air conditions using

$$Q_{0w} = \frac{T}{2\pi} \int_{-\omega_0}^{\omega_0} I_t d\omega, \tag{2}$$

132   where $-\omega_0$ and ω_0 represent the solar hour angles at sunrise and sunset, T is the

133   length of a day, and I_t is global irradiance.

134   **(2) Determination of GSR over rugged terrains**

135   The effects of aerosol, land surface factors (slope, aspect, terrain shading, and

136   surface cover), and cloud are considered in this part.

137   The daily GSR received on land surface consists of three parts (Fu, 1983).

138     $$Q_{\alpha\beta} = Q_{b\alpha\beta} + Q_{d\alpha\beta} + Q_{r\alpha\beta}, \tag{3}$$

139   where $Q_{\alpha\beta}$ is the daily GSR over rugged terrains, $Q_{b\alpha\beta}$ is the daily direct solar

140   radiation over rugged terrains, $Q_{d\alpha\beta}$ is the daily diffuse solar radiation over rugged

141   terrains, and $Q_{r\alpha\beta}$ is the daily reflected solar radiation over rugged terrains.

142   To determine $Q_{b\alpha\beta}$, we assume that

143     $$Q_{b\alpha\beta} = \frac{Q_{0\alpha\beta}}{Q_{0w}} Q_b = R_b Q_b, \tag{4}$$

144     $$Q_{b\alpha\beta} = Q_{0\alpha\beta} \frac{Q_b}{Q_{0w}} = Q_{0\alpha\beta} \frac{Q_b}{Q} \frac{Q}{Q_{0w}} = Q_{0\alpha\beta} f_b k_t , \tag{5}$$

145   where $Q_{0\alpha\beta}$ and Q_{0w} are the daily astronomical solar radiation over a terrain and a

146   horizontal surface, correspondingly, and Q_b is the direct solar radiation over a

147   horizontal surface. R_b represents the effects of slope, aspect, and topographic shadow,

148   Q is the daily GSR over a horizontal surface, f_b is the direct component coefficient,

149   and $k_t = a_G + b_G s$ (where s is the percentage of sunshine duration，and a_G and b_G are

150   empirical coefficients) is the clear sky coefficient. The effects of aerosol and cloud

151   are considered in the term $a_G + b_G s$.

152   Similar to Eq. (5), we derive an expression for the diffuse component.

153     $$Q_{d\alpha\beta} = Q_d [f_b k_t R_b + V(1 - f_b k_t)], \tag{6}$$

154   where Q_d is the diffuse solar radiation in the horizontal surface, and V is the terrain

155   openness (terrain openness + terrain shading = 1). The method for determining V is

156   described by Qiu (2003).

157        $Q_{0\alpha\beta}$ is calculated using Qiu's (2003) model, and Q_b and Q_d are calculated on the

158   basis of the empirical model exhibited by daily direct solar radiation and diffuse solar

159   radiation in the radiation station considering the effects of aerosol and cloud.

160   Finally, the reflected radiation from the sloped surface can be computed by the

161   following expressions:

162
$$\begin{cases} Q_{r\alpha\beta} = Q\rho_g(1-V) & V <= 1 \\ Q_{r\alpha\beta} = 0 & V > 1 \end{cases},$$
(7)

163   where ρ_g is the surface albedo, which can be retrieved from Landsat TM5 and

164   MODIS09GA. ρ_g is described in detail in Appendix.

165   **2.3.2. SEBAL model principle**

166   The SEBAL procedure consists of a series of algorithms. In this study, this

167   procedure is implemented using the ModelMaker module of ERDAS software. The

168   algorithms solve the complete energy balance equation

169        $$\lambda ET = R_n - G - H,$$
(8)

170   where λET is the latent heat flux, R_n is the surface net radiation flux, G is the oil

171   heat flux, and H is the sensible heat flux.

172   The parameterization of R_n and G is mature. Thus, the core issue of the model

173   is calculating H and ET. SEBAL model introduces a Monin-Obukhov loop iteration

174   to estimate H.

175   The above mentioned instantaneous results (H , R_n ,and G_0) are substituted in the

176   energy balance Eq. (8)   to calculate instantaneous latent heat flux λET . The daily

177   time scaling extension of the model is implemented on the basis of the evaporative

178   fraction (EF) method.

$$179 \qquad \frac{\lambda ET}{R_n - G} = EF , \qquad\qquad\qquad\qquad (9)$$

180   Following Shuttleworth et al., (1989), the instantaneous EF is assumed to be

181   similar to its 24 h counterpart (Brutsaert et al., 1992; Crago, 1996) and the assumption

182   supported by numerous field studies (Bastiaanssen et al., 1998a, b; Morse et al.,

183   2000).

184   Soil heat flux for 24 h periods is assumed to be nearly 0 for vegetated surfaces

185   given the canceling effect of positive G during daylight and negative G during

186   nighttime. Therefore, an actual λET_{24} for the 24-h evaporation can be computed as

$$187 \qquad \lambda ET_{24} = EF \times R_{n24} , \qquad\qquad\qquad\qquad (10)$$

188   where R_{n24} is the daily net radiation. The accuracy of the daily GSR estimation

189   largely determines the accuracy of R_{n24} estimation.

190   **2.3.3. Combination of multi-source remote sensing data for ET simulation**

191   Liu (2008) conducted a sensitivity analysis of the SEBAL model and suggested

192   that the LST and emissivity are highly sensitive to the simulated ET, whereas the

193   surface albedo, wind speed, NDVI, and aerodynamic roughness of a surface are

194   slightly sensitive to ET.

195   Only MODIS data can be used to calculate the daily ET because no TM data

196 from June 21 to 23, 2009, are available. Therefore, a co-simulation experiment on the

197 ET simulation, which uses three strategies of land surface parameters, is performed in

198 the present study. TM strategy refers to all the land surface parameters retrieved by

199 the TM image. MODIS strategy refers to all the land surface parameters retrieved by

200 the MODIS image. The TM/MODIS hybrid strategy, which combines the advantages

201 of the first two methods, refers to the LST from the MODIS11A1 image and the

202 surface albedo and NDVI from the TM image. The addition of the TM surface albedo

203 and NDVI can improve spatial resolution, whereas adding the MODIS LST can

204 improve temporal resolution. We can approximate that no change will occur in the

205 surface albedo and NDVI within a few days.

206 The TM image cycle is 16 days with a high spatial resolution, whereas the

207 MODIS image cycle is 1 day. However, the spatial resolution is less than the TM

208 image. Many local features retrieved by the TM image are generalized in the image

209 retrieved by MODIS. The TM/MODIS hybrid combines the advantages of the

210 spatiotemporal resolution of both strategies.

211 ## 3. Results and discussion

212 ### 3.1. Daily GSR

213 ### 3.1.1. Accuracy of simulated result

214 The validation results of the two models are summarized in Table 1. The mean

215 absolute bias error (MABE) of the improved daily GSR model is 9 W/m^2, and the

216 mean absolute relative bias error (MARBE) is 2.5%. The MABE of the daily GSR in

217   the SEBAL model is 122.2 W/m^2, and the MARBE is 33.9%.

218   The results show that the GSR on June 24, 2009, calculated in the SEBAL model

219   ranged from 438 W/m^2 to 465.7 W/m^2 with a mean of 446 W/m^2, which was much

220   higher than the improved daily GSR model with a range of 350–394 W/m^2 and a mean

221   of 370 W/m^2.

222   In Eq. (7), the surface albedo is calculated by two remote sensing data. The result

223   indicates that a slight difference of 0.4 W/m^2 in the daily GSR emerges by using the

224   surface albedo from the TM and MODIS images on June 24, 2009.

225   **3.1.2. Spatial pattern of daily GSR**

226   Theoretically, the GSR is larger on a sunny slope (an open place) than on a shady

227   slope (a rugged place), thereby indicating that the daily GSR is large where the

228   sunshine duration is long.

229   The spatial distribution of the daily GSR calculated using the SEBAL model

230   presents discontinuous and improper stripes (Fig. 3a). However, the calculation of the

231   improved model is more reasonable, because the effects of the spatial position

232   relations, percentage of sunshine, slope, aspect, terrain shading, and atmospheric

233   influence are comprehensively reflected.

234   An obvious difference between the SEBAL and the improved models is observed

235   in the southern area and the Longshou Mountain (Fig. 3b). The daily GSR in the

236   SEBAL model has reached the maximum value in the two areas. However, the daily

237   GSR in the improved model is near the minimal value. This result can be attributed to

238   the terrain shading that included a diffuse and reflected solar radiation in the new

model. In addition, the percentage of sunshine is higher in the northwest, thus implying that sunshine duration is long, and the corresponding daily GSR is high (Fig. 3b). However, these distribution features are unclear in the daily GSR in the SEBAL model.

The daily GSR of 0°, 45°, 90°, and 360° in the slope direction of the study area are statistically analyzed, and then the mean value is calculated (Fig. 4). In terms of local surface distribution pattern, the daily GSR must reach the maximum value near the south slope at 180°. However, the simulated results using the SEBAL model show that the daily GSR is only the minimum value (Fig. 4a), and the error is corrected by the improved model (Fig. 4b).

Therefore, the improved daily GSR model improves the calculation accuracy and makes the spatial distribution more reasonable than the original model.

3.2. Daily ET

3.2.1. Accuracy of simulated Daily ET

The comparative analysis of oasis stations (farmland [plain area]) is listed in Tables 2 and 3. The accuracy of the daily ET is higher in the improved scheme than in the original scheme, and ET is near the measured ET. The results show that the improved scheme using the TM/MODIS hybrid strategy is the optimum among the three models.

The simulated ET analysis of the TM/MODIS hybrid strategy of oasis stations from June 21 to 24, 2009, is summarized in Table 4. The mean measured ET for 4 days was 4.8 mm. The MABE of the improved scheme-simulated ET is 0.6 mm, and

the MARBE is 12%. For the original scheme ET, the MABE is 1.85 mm, and the MARBE is 39%. The mean ET of the wetland station (saline land) in 4 days is 2.2 mm. The simulated ET changes from 3.5 mm (original scheme) to 2.2 mm (improved scheme).

According to the research purpose and China's land use classification system, the study area is divided into 22 underlying surface coverage types (Fig. 2). Therefore, the TM/MODIS hybrid strategy of the original and improved schemes are used to calculate the ET of the 23rd and 24th days, respectively. The mean ETs of the two days in each surface coverage type are calculated and listed in Table 5. The mean measured ET for the two days is 4.6 mm in the farmland station. It changes from 6.3 mm (original scheme) to 4.3 mm (improved scheme). The mean measured ET for the two days is 2.2 mm in the wetland station. It changes from 3.7 mm (original scheme) to 2.4 mm (improved scheme).

In Table 5, the highest ET value has appeared in all types of water bodies, followed by farmland, forest, wetland, and residential areas. The ET values in the Gobi Desert and bare rock land are low. The water consumption in these areas is dominated by agriculture. The mean daily water consumption in the study area is $1.46 \times 10^7 \, \text{m}^3$. The farmland, which accounts for 44.8%, has consumed $6.5 \times 10^6 \, \text{m}^3$ in the improved scheme, and $9.5 \times 10^6 \, \text{m}^3$ in the original scheme.

3.2.2. Spatial pattern of daily ET

Figs. 5 and 6 illustrate that, for all land cover types, except for water bodies, the highest ET value is found over the farmland given the presence of irrigation water. In

283 addition, the ET is low in the area around the oasis. The differences in ET over the

284 various land types mainly depends on the NDVI. A large NDVI value indicates a high

285 ET.

286   In Fig. 5 and 6, the simulation ET based on the improved scheme declines more

287 than the original scheme. In the improved scheme, the desert ET is mainly distributed

288 in the vicinity of 0 mm, and the oasis ET is in the vicinity of 4.8 mm. In the original

289 scheme, the desert ET is mainly distributed in the vicinity of 0 mm, and the oasis ET

290 is in the vicinity of 6.5 mm.

291   The TM strategy has the highest resolution (Figs. 5a and 6a), whereas the

292 MODIS strategy has the lowest (Fig. 5b and 6b); many features retrieved by the TM

293 strategy are generalized in the image. The TM/MODIS hybrid strategy (Fig. 5c and 6c)

294 combines the advantages of the spatiotemporal resolution of both strategies to provide

295 a feasible scheme for the estimation of the daily ET on improving temporal resolution

296 and maintaining a relatively detailed spatial resolution.

297   Figs. 5a and 6a are images with cloud and cloud shadows at the northwest

298 corner, correspondingly. Several parts of the LST image in Figs. 5b and 6b are

299 missing; this phenomenon mostly occurs in desert areas. These areas are smaller than

300 the entire study area and cannot affect the statistical characteristics of various types of

301 land ET.

4. Conclusions

303   The new model fully considers the atmospheric and surface factors, especially

304 the influence of terrain shading on diffuse solar radiation and reflected solar radiation

305 over rugged terrains.

306   In order to estimate daily ET accurately, a new method for estimating the daily

307 GSR over the rugged terrains in the middle reaches of the Heihe River Basin is

308 proposed in this study. This method is based on Iqbal model C, fully considering the

309 atmospheric and surface factors, especially the influence of terrain shading on diffuse

310 solar radiation and reflected solar radiation over rugged terrains. The daily surface ET

311 on June 21–24, 2009, is simulated by using the SEBAL model, and a portion of the

312 daily GSR in the SEBAL model is improved. The results can be summarized as

313 follows:

314   The improved daily GSR with a resolution of 100 m×100 m is implemented; the

315 MABE of the simulated results is 9 W/m^2, and the MARBE is 2.5%. The MABE of

316 the daily GSR in the SEBAL model is 122.2 W/m^2, and the MARBE is 33.9%.

317   Theoretically, the spatial distribution of the daily GSR is more reasonable using

318 the improved model than the original model. The GSR is larger on a sunny slope (an

319 open place) than on a shady slope (a rugged place). In addition, if the percentage of

320 sunshine in the northwest is high, then the daily GSR is also high. The estimated

321 result of the improved daily GSR model is consistent with the distribution law, but the

322 estimated result of the SEBAL daily GSR model cannot fully reflect.

323   The co-simulation experiment on the ET simulation is designed for three

324 strategies, namely, TM, MODIS, and TM/MODIS hybrid strategies. They are used in

325 the original SEBAL model (original scheme) and the improved daily GSR SEBAL

model (improved scheme). The results show that the improved scheme ET is more accurate than the original scheme. Moreover, the TM/MODIS hybrid strategy in the improved scheme is the most reasonable in terms of accuracy and spatial distribution.

The simulated ET declines more based on the improved scheme than based on the original scheme. The mean measured ET of the oasis station in 4 days is 4.8 mm. The original scheme ET is 6.9 mm, and the improved scheme ET is 4.2 mm using the TM/MODIS hybrid strategy. The MABE of ET decreases from 2.1 mm (original scheme) to 0.6 mm (improved scheme), and the MARBE declines from 44% to 13% accordingly. And in all schemes desert ET is mainly distributed in the vicinity of 0 mm.

All simulated ETs show that the highest ET value is found in farmland, except for water bodies considering the presence of irrigation water, followed by farmland, forest, wetland, and residential areas, the lowest values appeared over bare rock land.

Different combination strategies show that the TM strategy has the highest resolution, and the MODIS strategy has the lowest; however, the TM image cycle is 16 days, whereas the MODIS image cycle is 1 day. The TM/MODIS hybrid strategy combines the advantages of the spatiotemporal resolution of both strategies.

During the growing season, the surface albedo and the height of the vegetation change daily. The calculation of ET is influenced by the satellite image quality, and the clouding images cannot be used. Thus, simulating continuously is difficult, especially using the TM/MODIS hybrid scheme. An approach that combines the ET estimates obtained from the TM with the drainage lysimeters has been verified useful

348   in computing cumulative ET (Morse et al., 2000).

349   In the growing season, the water of Heihe River is mainly consumed in the

350   middle reaches. Therefore, accurate calculation of water consumption of various land

351   types in the middle reaches, especially agricultural production, can effectively use

352   limited water resources, leave more water to the downstream, and make the

353   downstream ecological environment better.

354   **Appendix**

355   **MODIS09GA**

356   Broadband shortwave surface albedo is calculated from the normalized reflection

357   values of Channels 1, 2, 3, 4, 5, and 7 using the following equation (Liang et al.,

358   2003):

359    $\rho_g = 0.160\alpha_1 + 0.291\alpha_2 + 0.243\alpha_3 + 0.116\alpha_4 + 0.112\alpha_5 + 0.081\alpha_7 - 0.0015$.   (1)

360   **TM5**

361    $\rho_g = \dfrac{\alpha_{toa} - \alpha_{path\_radiance}}{\tau_{sw}^2}$,   (2)

362   where α_{toa} is the atmospheric top reflectivity and can be obtained from the weighted

363   average of the reflectivity of the shortwave bands (1, 2, 3, 4, 5, and 7 bands of TM) in

364   remote sensing images. $\alpha_{path\_radiance}$ is the albedo path radiance, and τ_{sw}^2 is the

365   two-way transmittance (Morse et al., 2000).

References

Teixeira AH de C, Bastiaanssen WGM, Ahmad MD, Bos MG: Reviewing SEBAL input parameters for assessing evapotranspiration and water productivity for the Low-Middle Sao Francisco River basin, Brazil Part A: Calibration and validation. Agr Forest Meteorol 149,462-476. https://doi.org/10.1016/j.agrformet.2008.09.016,2009

Bastiaanssen WGM, Menenti M, Feddes RA, Holtslag AAM:The Surface Energy Balance Algorithm for Land (SEBAL): Part 1 formulation, Journal of Hydrology 212-213: 198-212, 1998a.

Bastiaanssen WGM, Pelgrum H, Wang J, Ma Y, Moreno J, Roerink GJand van der Wal T : A remote sensing Surface Energy Balance Algorithm for Land (SEBAL): Part 2 validation. J. Hydr. 212-213,213-229,(1998b.

390   Bastiaanssen WGM, Noordman EJM,Pelgrum H,Davids G,Thoreson BP,Allen RG: SEBAL

391   model with remotely sensed data to improve water-resources management under actual

392   field conditions. J. Irrig. Drain. Eng. 131(1), 85-93,2005.

393   Brutsaert W, Sugita M:Application of Self-Preservation in the Diurnal Evolution of the

394   Surface Energy Budget to Determine Daily Evaporation. J. Geophys. Res. 97,

395   18377-18382. http://dx.doi.org/10.1029/92JD00255, 1992.

396   Crago RD: Conservation and variability of the evaporative fraction during the

397   daytime.J.Hydrol.,180,173-194,1996.

398   Fu B P:Mountain Climate. Beijing Science Press 270 pp,1983.

399   Iqbal M:An Introduction to Solar Radiation. Academic Press 390 pp, 1983.

400   Kite GW: Using a basin-scale hydrological model to estimate crop transpiration and soil

401   evaporation. J. Hydr 229:59-69,2000.

402   Li SB, Zhao WZ: Satellite-based actual evapotranspiration estimation in the middle reach of

403   the Heihe River Basin using the SEBAL method. Hydrol. Process 24, 3337-3344. doi:

404   10.1002/hyp.7748,2000.

405   Liang S, Shuey CJ, Russ AL,et al.: Narrowband to broadband conversions of land surface

406   albedo.J. II -Validation. Remote Sens. Environ 84(l):25- 41,2000.

407   Liu CS Regional Land Surface Water/Heat Flux Modeling and Application Based on Remote

408   Sensing in Shandong Province. Phd. thesis, Nanjing University of Information Science &

409   Technology, 2008.

410   Markham B, Barker J: Landsat MSS and TM post-calibration dynamic ranges,

411   exo-atmospheric reflectances and at-satellite temperatures. Landsat Technical Notes,

1986.

Mobin-ud Din Ahmad, Mac Kirby, Mohammad Shahidul Islam,et al.: Groundwater Use for Irrigation and its Productivity: Status and Opportunities for Crop Intensification for Food Security in Bangladesh. Water Resour Manag 28(5), 1415-1429.doi: 10.1007/s11269-014-0560-z, 2014.

Morse A, Tasumi M, Allen RG, Kramber WJ:Application of the SEBAL methodology for estimating consumptive use of water and streamflow depletion in the Bear River Basin of Idaho through Remote Sensing. Final Report Submitted to The Raytheon Systems Company Earth Observation System Data and Information System Project, 2000.

Usman M, Liedl R, Awan UK: Spatio-temporal estimation of consumptive water use for assessment of irrigation system performance and management of water resources in irrigated Indus Basin. Pakistan. J. Hydrol 525,26–41. https://doi.org/10.1016/j.jhydrol.2015.03.031, 2015.

Nie ZL: Study on Groundwater Circulation and Renewability in the Middle Reaehes of Heihe River Valley,Northwest China. Phd. thesis, Chinese Academy of Geological Sciences,2004.

Qiu XF: Distributed Modeling of Solar Radiation Over Rugged Terrains. Phd. thesis, Nanjing University, 2003.

Rahman M, Sulis M, Kollet SJ: Evaluating the dual-boundary forcing concept in subsurface– land surface interactions of the hydrological cycle. Hydrol. Process 30,1563-1573. https://doi.org/10.1002/hyp.10702,2016.

Sellers PJ, Randall DA, Collatz CJ, et al.: A revised land surface parameterization (SiB2) for

434   atmosphere GCMs. Part I: Model formulation. J Climate 9: 676-705, 1996.

435   Shuttleworth WJ, Gurney RJ, Hsu AY, Ormsby JP: FIFE:The variation in energy partition at

436   surface flux sites. In A.Rango(Ed.),Remote sensing and large-scale processes (Proceeding

437   of   the   IAHS   third   internation   Assembly,Baltimore,MD,May,1989).   IAHS

438   Publication,vol.186.(pp.66-74) ,1989.

439   Shi GP,Qiu XF,Zeng Y: New Method for Estimating Daily Global Solar Radiation over

440   Sloped   Topography   in   China.   Adv.   Atmos.   Sci   35(3),   285   –

441   295.https://doi.org/10.1007/s00376-017-6243-y,2018.

442   Chen X, Su Z, Ma Y, Yang K, Wang B: Estimation of surface energy fluxes under complex

443   terrain of Mt. Qomolangma over the Tibetan Plateau. Hydrol. Earth Syst. Sci 17, 1607–

444   1618. doi:10.5194/hess-17-1607-2013,2013

445   Yin JQ: Study on daily evapotranspiration estimation model by remote sensing coupling daily

446   global solar radiation model and daily mean LST model. Phd. thesis, Nanjing University

447   of Information Science & Technology ,2014.

448   Yin JQ, Qiu XF, He YJ: Modelling the spatial and temporal variation laws of Diffuse Solar

449   Radiation of Rugged Terrain over Zhejiang Province. Transcations of Atmospheric

450   Sciences 34(1),93-98,2011.

451   Yeom J M, Seo Y K, Kim D S, Han KS: Solar radiation received by slopes using COMS

452   imagery, a physically based radiation model, and GLOBE. J.Sensors 2016, 4834579,

453   https://doi.org/10.1155/2016/4834579,2016.

454   Zeng Y,Qiu XF, Liu SM: Distributed modeling of extraterrestrial solar radiation over rugged

455   terrains. Chin J. Geophys-ch 48(5), 1028-1033,2005.

456

457 **Figures**
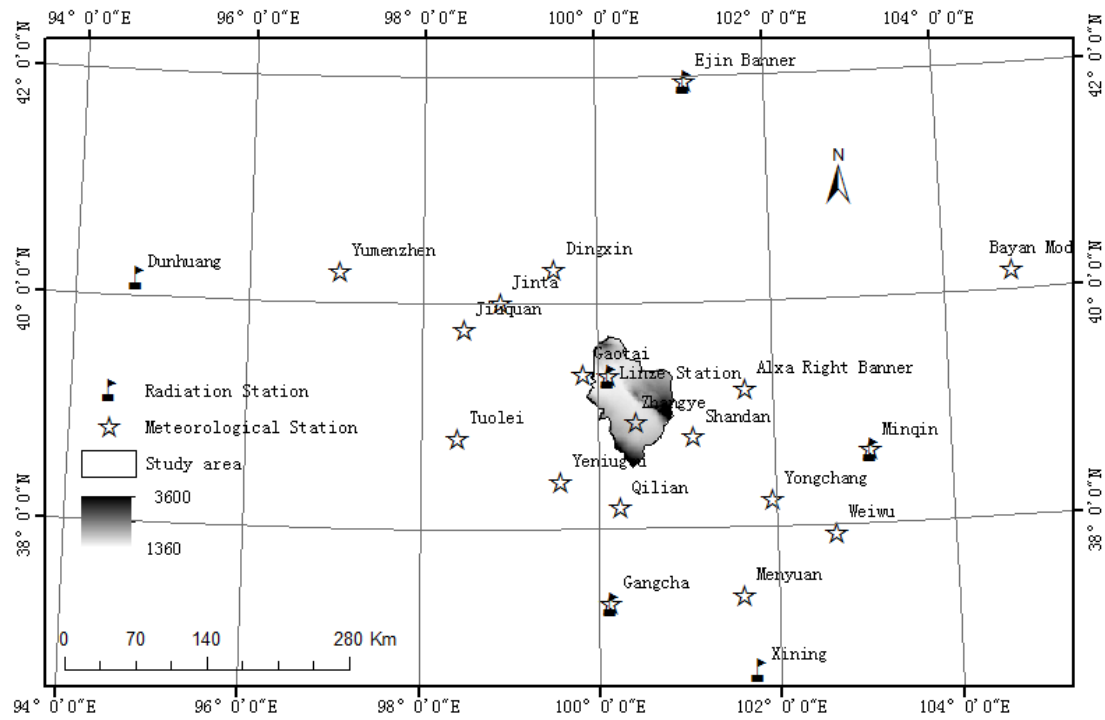
459 Fig.1. Distribution of meteorological stations and DEM of the middle reach of the Heihe

460 River (unit: m)

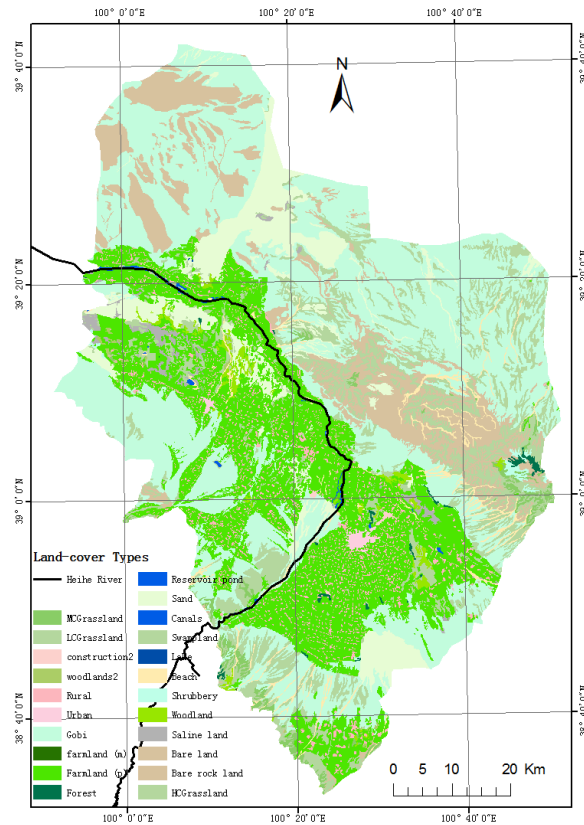461

462

463

464   Fig.2. Land-cover map of the study area

465   (High-coverage grassland: HCGrassland, Moderate-coverage grassland: MCGrassland,

466   Low-coverage grassland: LCGrassland, Sand desert: Sand, Gobi desert: Gobi, Other

467   woodlands:woodlands2, Other construction:construction2, Rural residential: Rural, farmland

468   (mountain):Farmland (m), Farmland (plain):Farmland(P))

469

470
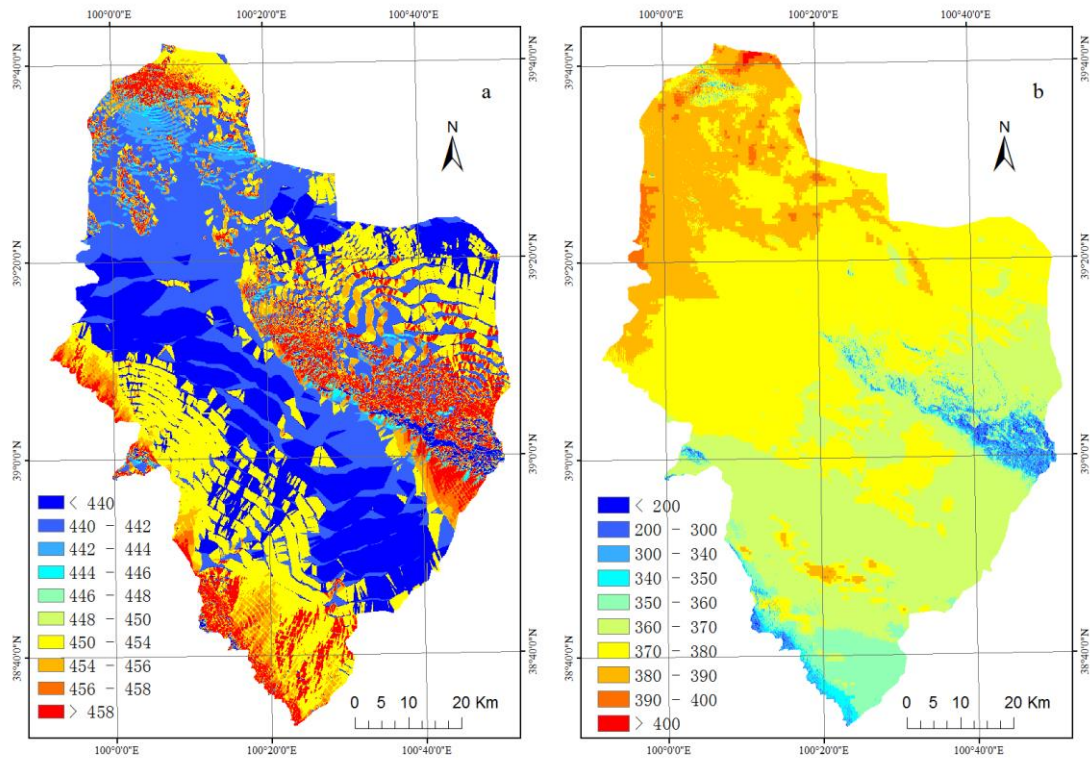
471   a.original SEBAL model   b.improved model

472   Fig.3. Spatial distribution of daily GSR in the middle Heihe River Basin on 24 June,

473 2009 (Unit: W/m^2)

474

475

476

477

478

479

480

481

482

483

a. Aspect (degree)

484

b. Aspect (degree)
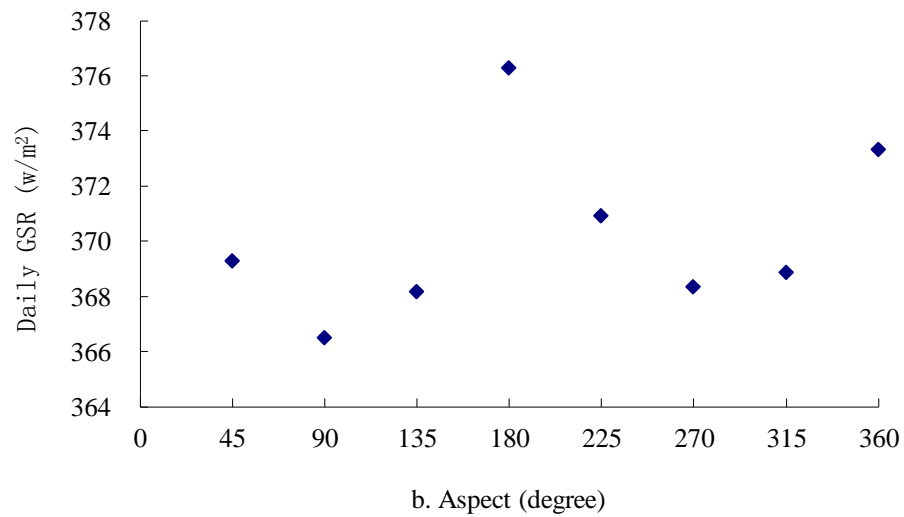
485
486   Fig.4. Relation between daily GSR and aspect in the middle Heihe River Basin on 24 June,
487   2009 (Unit: mm)
488   (a. original SEBAL model, b. improved model)

489

490

491   a. TM strategy   b. MODIS strategy
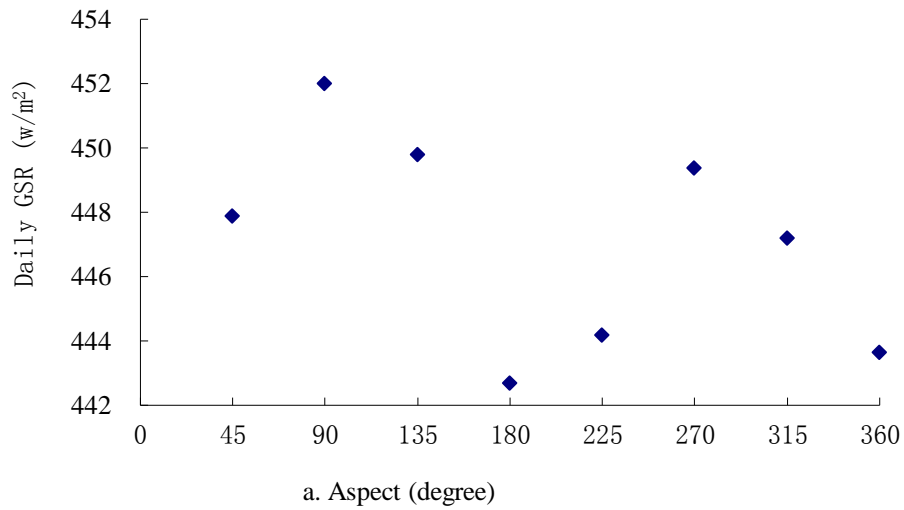

492
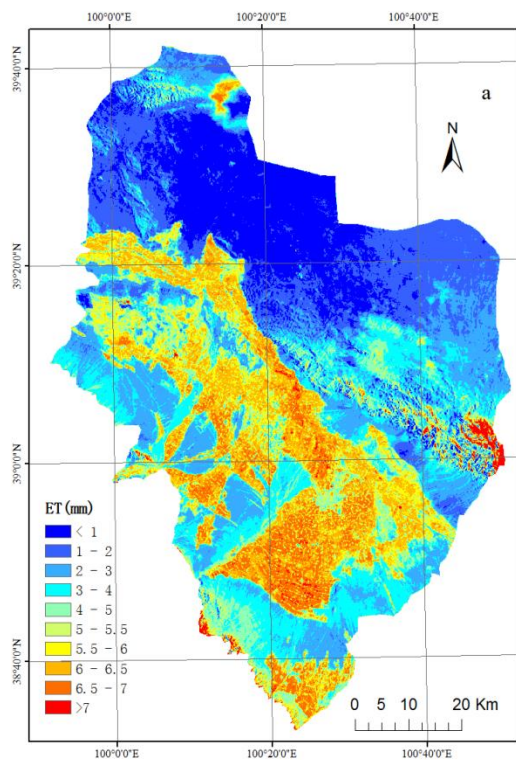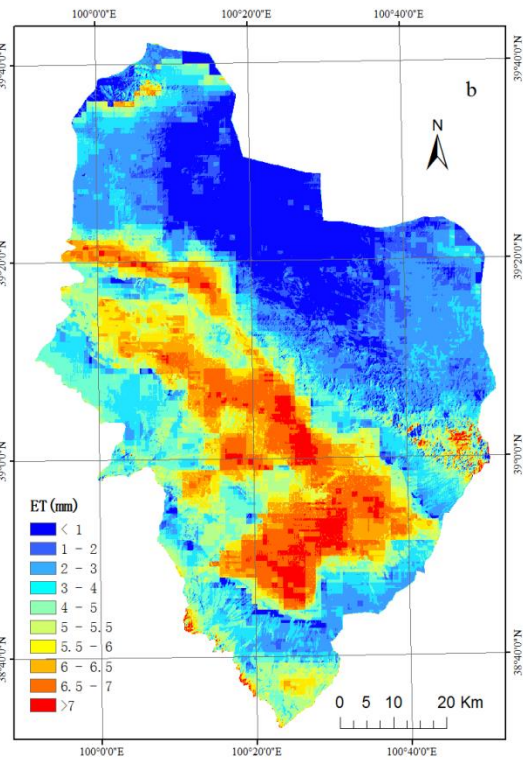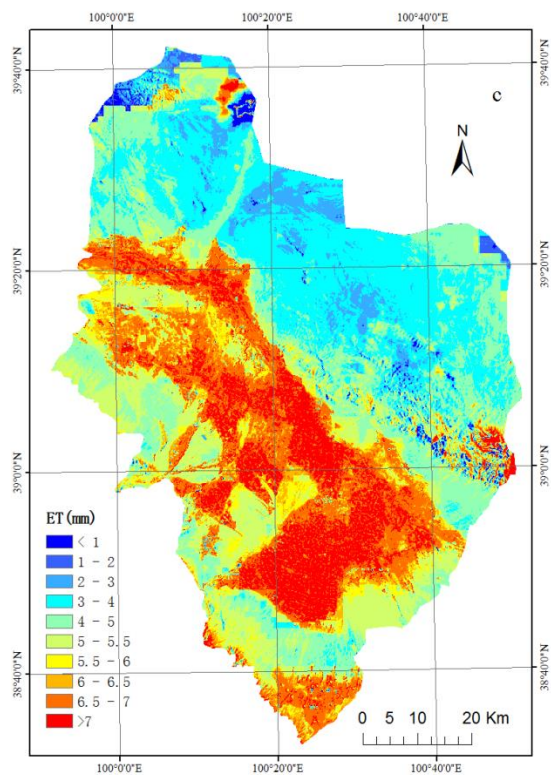
493   c.   TM/MODIS hybrid strategy

494   Fig.5. Spatial distribution of ET retrieved using original scheme on 24 June, 2009 (Unit:

495   mm)

496

497   a. TM strategy   b. MODIS strategy

498
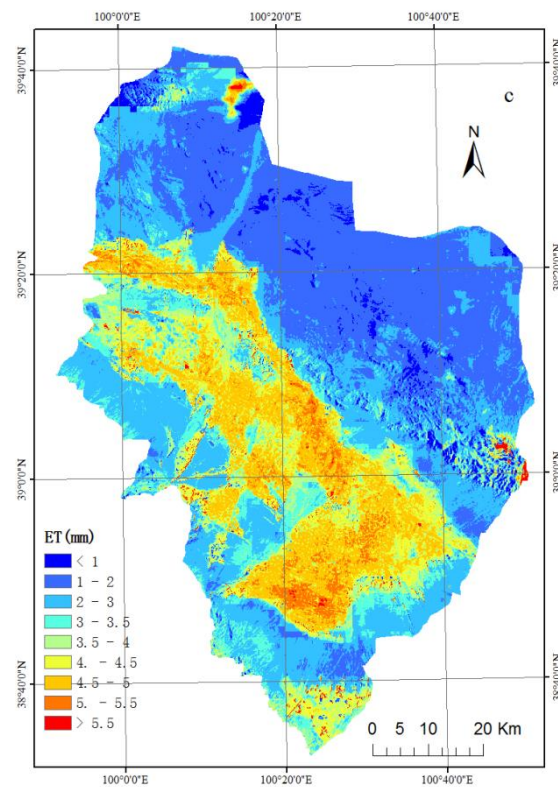
499   c.   TM/MODIS hybrid strategy

500   Fig.6. Spatial distribution of ET retrieved using improved scheme on 24 June, 2009 (Unit:

501   mm)

502 **Tables**

503 Table 1

504 Daily GSR of middle Heihe River Basin on June 21–24, 2009 (Unit: W/m^2)

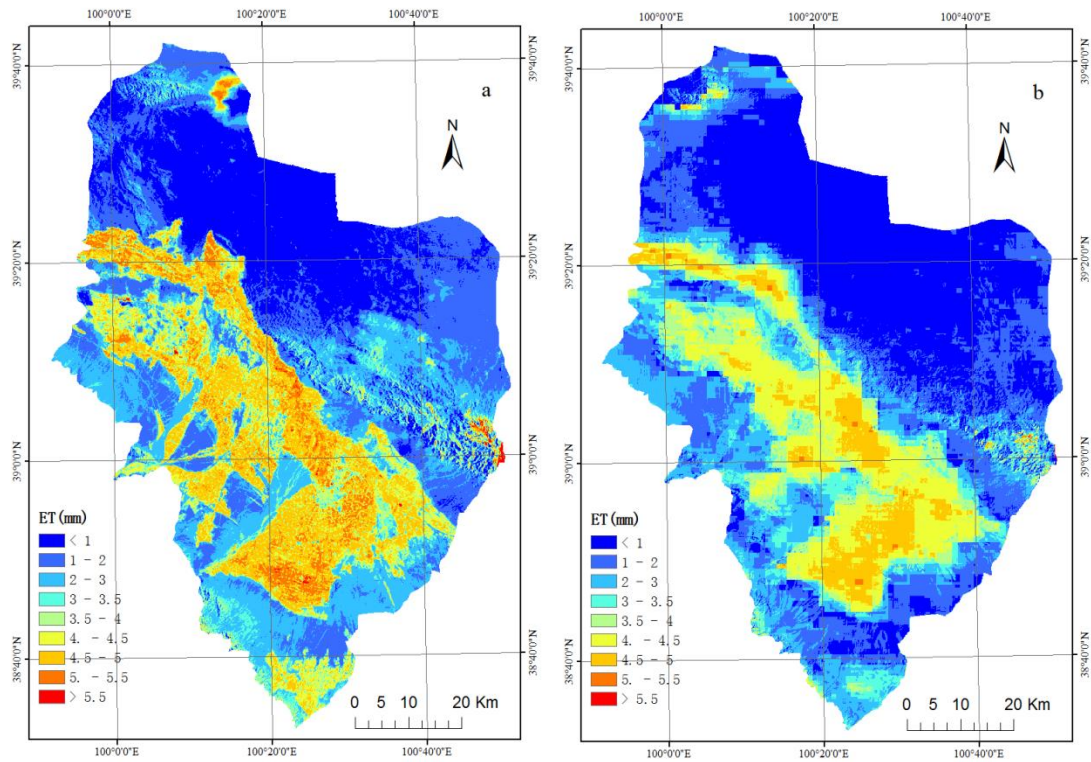| Date	measure daily GSR	simulated daily GSR		MABE		MARBE（%）	
		improved	original	improved	original	improved	original
6.21	354.2	346.1	484	8.1	129.8	2.3	36.6
6.22	360	355.3	484.1	4.7	124.1	1.3	34.5
6.23	377.3	375	484.3	2.3	107	0.6	28.4
6.24	356.5	377.3	484.4	20.8	127.9	5.8	35.9
Mean	362	363.4	484.2	9	122.2	2.5	33.9

505
506
507
508
509
510
511
512
513
514
515
516
517
518
519
520
521
522
523
524
525
526
527
528
529
530
531
532
533
534
535
536

537 Table 2

538 ET of three combination schemes on 24 June, 2009(Unit: mm)

Classification	measured ET	original scheme	improved scheme
TM strategy	4.8	6.3	5.0
MODIS strategy	4.8	6.3	4.2
TM/MODIS Hybrid strategy	4.8	7.0	4.8

539

540

541

542

543

544

545

546

547

548

549

550

551

552

553

554

555

556

557

558

559

560

561

562

563

564

565

566

567

568

569

570

571

572

573

574

575 Table 3

576 Errors of ETs of three combination strategies on 24 June, 2009(Unit: mm)

simulation strategy	simulation scheme	MABE	MABRE (%)
TM strategy	original scheme	1.5	31
	improved scheme	0.2	4
MODIS strategy	original scheme	1.5	31
	improved scheme	0.6	13
TM/MODIS strategy	original scheme	2.2	46
	improved scheme	0	0

577
578
579
580
581
582
583
584
585
586
587
588
589
590
591
592
593
594
595
596
597
598
599
600
601
602
603
604
605
606
607

608 Table 4

609 Daily ET of middle Heihe River Basin on June 21–24, 2009 (Unit: mm)

Date	Measure ET	simulated ET		MABE		MARBE（%）	
		improved	original	improved	original	improved	original
6.21	4.9	3.8	6.6	1.1	1.7	22	35
6.22	5.1	3.9	6.5	1.2	1.4	24	27
6.23	4.5	4.4	6.6	0.1	2.1	2	47
6.24	4.8	4.8	7	0	2.2	0	46
Mean	4.8	4.2	6.7	0.6	1.85	12	39

610

611

612

613

614

615

616

617

618

619

620

621

622

623

624

625

626

627

628

629

630

631

632

633

634

635

636

637

638

639

640 Table 5

641 ET of each land-cover types

Underlying Surface Type	Area (km^2)	improved scheme Mean ET (mm)	original scheme Mean ET (mm)
Forest land	16.43	3.5	5.6
Shrubbery	15.73	2.1	3.6
Woodland	56.99	3.4	5
Other woodlands	7.89	3.5	5.3
High-coverage grassland	36.43	3	4.9
Moderate-coverage grassland	76.43	2.5	4.2
Low-coverage grassland	731.89	1.9	3
Canals	20.24	4.5	6.6
Lake	0.16	3.6	5.4
Reservoir pond	4.2	4	5.6
Beach	106.18	2.1	3.2
Urban Land	15.33	3.8	5.5
Rural residential land	164.1	4	5.9
Other construction lands	4.51	3.8	5.6
Sand desert	472.64	1.4	2.3
Gobi desert	2321.37	1.4	2.1
Saline land	49.2	2.4	3.7
Swampland	4.48	4.2	6
Bare land	78.74	1.1	1.7
Bare rock land	558.52	1.5	2.3
farmland (mountain area)	0.13	3.7	5.9
Farmland (plain area)	1515.16	4.3	6.3

642

643

644